

# Capillary origami: spontaneous wrapping of a droplet with an elastic sheet

C. Py<sup>1</sup>, P. Reverdy<sup>2</sup>, L. Doppler<sup>1</sup>, J. Bico<sup>1</sup>, B. Roman<sup>1</sup> and C. N. Baroud<sup>2</sup>

<sup>1</sup> *Physique et Mécanique des Milieux Hétérogènes, ESPCI,*

*Paris 6, Paris 7, UMR CNRS 7635, 75231 Paris cedex5, France*

<sup>2</sup> *Laboratoire d'Hydrodynamique (LadHyX) and Département de Mécanique, École Polytechnique, UMR CNRS 7646, 91128 Palaiseau cedex, France*

(Dated: March 23, 2022)

**Abstract** The interaction between elasticity and capillarity is used to produce three dimensional structures, through the wrapping of a liquid droplet by a planar sheet. The final encapsulated 3D shape is controlled by tailoring the initial geometry of the flat membrane. A 2D model shows the evolution of open sheets to closed structures and predicts a critical length scale below which encapsulation cannot occur, which is verified experimentally. This *elastocapillary length* is found to depend on the thickness as  $h^{3/2}$ , a scaling favorable to miniaturization which suggests a new way of mass production of 3D micro- or nano-scale objects.

PACS numbers: 46.32.+x, 68.08.-p, 81.16.Dn, 85.85.+j

Origami and haute couture design both rely on folding and assembling planar material to create elegant three-dimensional (3D) shapes whose variety and complexity is governed by the number, order and orientation of folds. Folding is also a way to reduce the size of deployable structures in space industry (satellite pannels or sun sails [? ]) as well as in nature (plant leaves folded in a bud [? ]). In micro and nano-fabrication, the folding of planar structures is a promising approach to build 3D objects, since most microfabrication technologies produce planar layers through surface etching [? ].

While centimeter-sized objects may be folded using well disposed magnets [? ], capillarity is a particularly relevant mechanism for micro-fabrication [? ], as surface forces dominate over bulk forces at small scales. Indeed, the capillary attraction and stiction of wet slender structures may induce disastrous damage in micro and nano-scale fabrication [? ? ? ? ], in addition to being involved in lung airway closure (neonatal respiratory distress syndrome) [? ]. Capillary interactions have already been proposed as a way of assembling and orienting rigid objects in 2D at the surface of water [? ], or in 3D by capillary bridges [? ], while further studies have focused on the capillary induced deflection of elastic rods [? ? ? ]. Recently, the multi-folding of a flexible ribbon squeezed in a meniscus has also been described through an elegant experiment [? ]. Here, we address the effect of capillary forces on a flat elastic membrane and we show how the spontaneous folding of a flexible sheet around a liquid droplet leads to a predetermined 3D shape.

Our experiments were conducted using polydimethylsiloxane (PDMS) membranes. The PDMS (Dow corning Sylgard 184, 10:1 polymer/curing agent mix) was spin coated at 24°C on a glass microscope slide, at rotation rates of 1000-2000 rpm. Once the PDMS was cured, this resulted in sheets with thickness in the range 80-40  $\mu\text{m}$ .

During a typical experiment, a geometric shape is manually cut out from the PDMS layer and placed on a superhydrophobic surface. A drop of water, of volume 1–80  $\mu\text{L}$  depending on membrane size, is deposited on the PDMS,

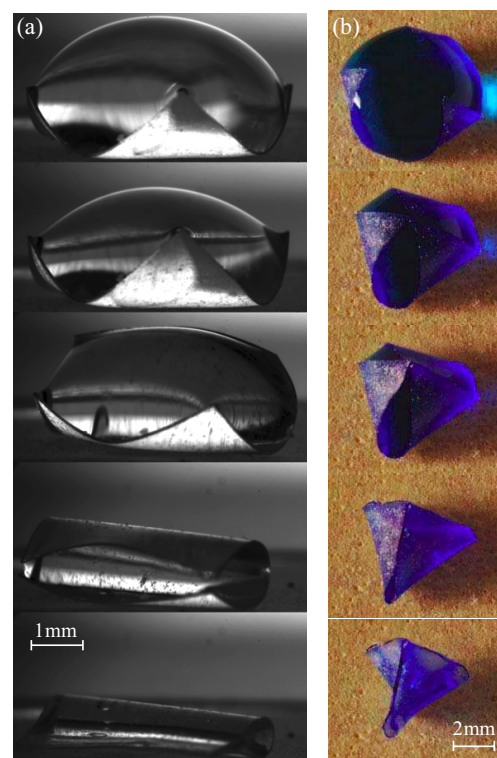


FIG. 1: Wrapping of a drop of water with (a) square and (b) triangular PDMS sheets. The total elapsed time for each experiment is about half an hour.

while making sure that the water reaches all the corners of the flat sheet. The water is then allowed to evaporate at room temperature and a time lapse sequence of images is taken of the membrane/drop pair. As the water volume decreases from its initial value to complete evaporation, the surface tension of the liquid pulls the sheet around smaller volumes, thus increasingly curving it (Fig. 1). Sufficiently thin sheets eventually encapsulate the liquid with a shape that depends on the initial cut of the membrane.

In the simplest case, a drop is deposited on a square PDMS sheet, as shown in Fig. 1a. This initially leads to the bending of the four corners towards the center (mode-4). As the drop volume decreases further, this bending mode becomes unstable and the shape rapidly switches to a mode-2 state; in this state, the corners are attracted to each other two by two and the flat central region disappears, giving rise to a quasi-cylindrical shape (middle image in Fig 1a). As the drop volume decreases further, the approaching edges eventually touch and a water-filled tube, a few hundred microns in diameter, is formed. Finally, the water evaporates completely and the tube enlarges into a loop whose ends merge into a flat contacting region, similar to the shape shown in Fig. 2a..

A different situation occurs when a drop is deposited on a triangular sheet, see Fig. 1b and Movie S1 ([www.pmmh.espci.fr/~benoit/wrapping.avi](http://www.pmmh.espci.fr/~benoit/wrapping.avi)). The corners fold towards the center as in the previous case, but this leads to a stable mode-3 folding. The three corners eventually join at the center and the sheet seals into a tetrahedral pyramid. At this stage, the curvature of the surface is concentrated on the edges of the pyramid, while the sides are almost flat (fourth image in Fig. 1b). Further evaporation, which now occurs at a slower rate, finally leads to the buckling of the pyramid walls due to the negative internal pressure (final image).

For both of the above geometries, the scenario is different for membranes of smaller size or larger thickness. As the stiffness increases, the forces generated by surface tension become insufficient to achieve complete closure: after going through similar initial stages as for thin PDMS layers, a maximum bending of the sheet is produced after which it reopens again, never having produced an encapsulated drop. The final state is therefore a planar sheet covered by a thin film of liquid which quickly evaporates.

The membrane deformations reduce the liquid-air area  $A$  and thus the surface energy  $\gamma A$  ( $\gamma$  being the surface tension), at the cost of increasing the elastic energy. For a thin plate, the isometric bending energy density is defined locally as  $B\kappa^2/2$ , where  $\kappa$  is the curvature and  $B = Eh^3/12(1 - \nu^2)$  is the bending stiffness ( $E$  is the Young's modulus,  $\nu$  is Poisson's ratio and  $h$  is the thickness) [? ]. For a system of typical dimension  $L$ , folding will occur if the surface energy ( $\gamma L^2$ ) is large compared to the total bending energy ( $B$ ). This is equivalent to comparing  $L$  to

$$L_{EC} = (B/\gamma)^{1/2}, \quad (1)$$

that we refer to as the *elastocapillary length* [? ]. Physically,  $L_{EC}$  gives the typical radius of curvature generated by capillary forces for a given bending rigidity.

The elastocapillary length can be measured directly through a calibration experiment rather than by estimating each parameter in Eq. 1 which would produce large errors. The experiment consists in depositing a drop of wetting liquid onto a very long strip of PDMS, which

folds over into a loop with a self-contacting tail. We consider the late stage, when only a small meniscus still holds the loop together (Fig. 2a).

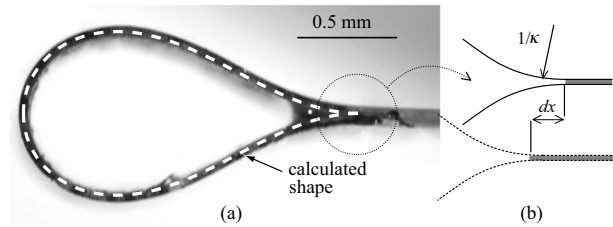


FIG. 2: (a) Experimental image of a loop of PDMS held by a meniscus of ethanol, and comparison with the rescaled theoretical shape (white curve). (b) Virtual displacement  $dx$  of the meniscus position.

This equilibrium state is 2D, so the following analysis is understood to be per unit depth. The cross-section follows planar rod elasticity coupled with surface tension. We note  $\theta(s)$  the angle made by the tangent to the rod  $\mathbf{t}$  with respect to the horizontal, at curvilinear coordinate  $s$ . We also note  $\mathbf{R}$  the constant vectorial tension of the beam, so that Euler's elastica equations for equilibrium may be expressed as [? ]

$$B \frac{d^2\theta}{ds^2} \mathbf{e}_z + \mathbf{t} \times \mathbf{R} = \mathbf{0}, \quad (2)$$

where  $\mathbf{e}_z$  is the unit vector perpendicular to the plane of the section. The global shape of the loop is determined by elasticity, given the curvature at the contact point. Since this curvature is set by an equilibrium between surface tension and elasticity, it must scale as  $1/L_{EC}$ . The prefactor is found by considering a virtual displacement  $dx$  of the contact point for a loop of curvilinear length  $2\ell$  (see Fig. 2b). The elastic energy,  $E_{el} = \int_{-\ell}^{\ell} B\kappa^2/2 ds$ , varies due to the change in the integral bounds, the integrand being stationary near elastic equilibrium. It may be written as  $dE_{el} = B\kappa_c^2 dx$ , where  $\kappa_c$  is the curvature at the contact point. On the other hand, the variation of surface energy due to replacing a solid-gas interface (surface energy  $\gamma_{SG}$ ) with a solid-liquid interface ( $\gamma_{SL}$ ) is  $2(\gamma_{SL} - \gamma_{SG})dx = 2\gamma \cos\alpha dx$ , where  $\alpha$  is the contact angle of the liquid on the surface (here we use ethanol which has a zero contact angle  $\alpha$  on the PDMS). Balancing the two energies yields the value of equilibrium curvature at the contact point:

$$\kappa_c = \frac{\sqrt{2}}{L_{EC}}. \quad (3)$$

The boundary value problem of Eqs. (2) and (3) was solved numerically by enforcing the contact condition at the base of the loop,  $\int_{-\ell}^{\ell} \sin(\theta) ds = 0$ , and  $L_{EC}$  was measured by scaling the numerical solution to fit the experimental shape. An excellent agreement is obtained (white

line superimposed on experimental picture in fig 2a). In practice the width of the loop (theoretical value  $0.89L_{EC}$ ) is sufficient to determine  $L_{EC}$ .

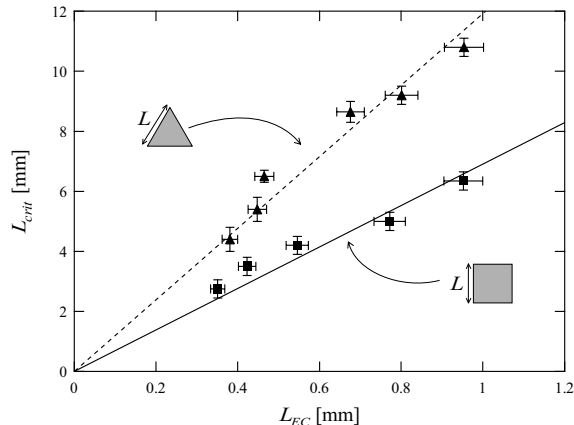


FIG. 3: Critical length for folding vs. elasto-capillary length: black squares: square sheets, black triangles: triangular sheets (leading to 3D pyramids), lines: linear regressions.

The value of  $L_{EC}$  was measured for different membrane thicknesses and for each thickness, the minimum length for encapsulation  $L_{crit}$  was determined for square and triangular membrane shapes. We found that  $L_{crit}$  varied linearly with  $L_{EC}$  for both shapes, as one might expect from dimensional arguments. The slopes were 7.0 for the squares and 11.9 for the triangles (Fig 3).

An understanding of the evolution of the folding is obtained from a 2D theoretical description of the elasto-capillary balance: let us consider an elastic inextensible rod of length  $L$  bent by pressure and surface tension forces at its ends (Fig. 4 inset). Equation (2) still holds but the vectorial tension  $\mathbf{R}$  is not constant anymore due to the pressure forces but follows

$$\frac{d\mathbf{R}}{ds} + p\mathbf{n} = \mathbf{0}, \quad (4)$$

where  $\mathbf{n}(\mathbf{s})$  is the unit vector normal to the rod. By neglecting gravity, the pressure  $p$  in the drop is uniform and the 2D shape of the liquid-air interface is a circular arc of radius  $r = \gamma/p$ .

Equations (2) and (4), with appropriate boundary conditions, are solved numerically and the distance  $\delta$  between the rod tips is calculated as a function of drop section area  $S$  for different rod lengths  $L$ , as shown in Fig. 4. Two trivial flat states ( $\delta/L = 1$ ) exist in all cases for an infinitely large drop (A and A') or when no liquid is present (B or B'). However, the evolution between these states is qualitatively different depending on  $L/L_{EC}$ .

For  $L/L_{EC}$  slightly below the critical value (Fig. 4a), these two states are connected by a continuous family of solutions: the drying of a large drop leads to transient limited bending but eventually to reopening. Closed

states (C) do exist in a restricted domain of the phase space, as the stable segment of a solution loop, while the unstable part of this loop corresponds to a drop which has depinned from the edges (D). This bistability is indeed observed in the experiments: while small sheets never close spontaneously, they can be forced into a closed state if the liquid is pulled out with a syringe.

Above the critical ratio  $L/L_{EC}$ , the drying of a large drop (A') leads continuously to complete wrapping (C'), as observed experimentally in Fig. 1. Another branch links the open state (B') to unstable solutions (D'). However, this branch is difficult to observe experimentally because it requires the spreading of a thin film of water on the flat membrane. Finally, figure 4 shows that the initial conditions play a major role in selecting the final observed state because of the presence of bistability.

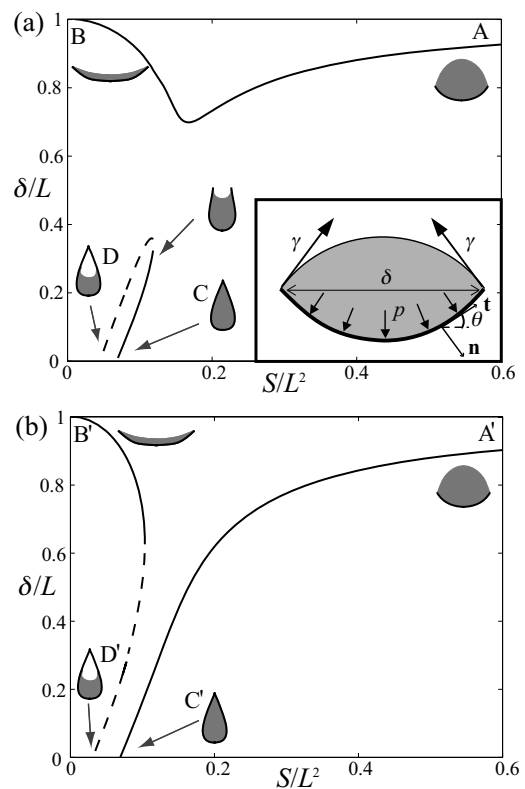


FIG. 4: Distance between the rod tips versus drop volume for different values of the rod length  $L$ : (a)  $L = 3.4L_{EC}$  reopening of the rod as  $S$  decreases; (b)  $L = 4L_{EC}$  complete wrapping of the rod around the drop. The inset shows a sketch of a 2D drop deposited on a flexible sheet.

In the numerical simulations, the crossing from diagrams (a) to (b) was found at  $L_{crit} = 3.54 L_{EC}$ . This is below the value obtained for the square membranes, even though the final state of a folded square is 2D (Fig. 1a). This discrepancy is likely due to gravity and 3D effects, neither of which is accounted for in the model. Indeed, the drops considered in Fig. 3 are slightly flattened by gravity, since they are larger than the capillary length

( $L_c = \gamma/\rho g$ , where  $\rho$  is the density and  $g$  the acceleration of gravity). More importantly, the early stages are always 3D as seen in the folding of the corners (e.g. mode-4 folding) and thus deviate the evolution from the prediction of the 2D model. A 3D theoretical model should include the full description of thin plate elasticity. Only such a model would account for the localization of the curvature around the edges of the pyramid for example, which are reminiscent of the crumpling of thin sheets.

More generally, 3D wrapping of a droplet leads to a geometrical incompatibility described by Gauss's *theorem egregium*. A classic example is that it is impossible to draw a planar map of the earth which conserves distances: the wrapping of a spherical object with a planar sheet must involve stretching as well as bending. For a thin membrane, the stretching energy scales as the thickness  $h$  and is therefore much more expensive than the bending energy which scales as  $h^3$ . The unavoidable stretching is therefore localized in singular regions, leading to crumpling singularities [? ? ]. We expect that for  $L \gg L_{EC}$ , the number of singularities will increase since surface tension becomes dominant over elastic forces, leading to quasi-spherical encapsulated shapes.

Precise engineering of the final closed state may be obtained by tailoring the initial sheet geometry. In this way, it is possible to approximate a smooth sphere by starting with a flower shape, as shown in Fig. 5a. Figure 5b shows how to form a cube by starting from a cross shape. As in the case of the pyramid, evaporation

after encapsulation takes place at a reduced rate and may buckle the sphere or the cube due to the negative pressure thus generated. However, one may also freeze (or polymerize) the encapsulated liquid at any point in this process, therefore fixing the desired shape in place. Finally, small perturbations of the initial shape may also be used to yield different final states. In particular, rounding-off two opposite corners of a square sheet leads to the membrane closing along its diagonal (Fig. 5c) rather than parallel to the sides. These experiments suggest that a wide variety of final shapes may be achieved through careful tuning of the initial 2D shape.

In summary, three dimensional sub-millimetric objects are produced from 2D membranes through the interaction of elasticity and capillarity. The limitation on the minimal size for folding is determined by the elastocapillary length (Eq. 1) which scales as the sheet thickness  $h^{3/2}$ . This scaling is favorable to miniaturization since thinner membranes lead to much smaller critical lengths. This opens the way to mass production of micron-scale 3D structures based on standard microfabrication methods since a wide variety of objects can be fabricated by tailoring the initial planar sheet.

We are very grateful to Emmanuel de Langre (Lad-HyX, Ecole Polytechnique) for his important insights. This work was partially supported by the French ministry of research (ACI *Structures élastiques minces*), and the Société des Amis de l'ESPCI.

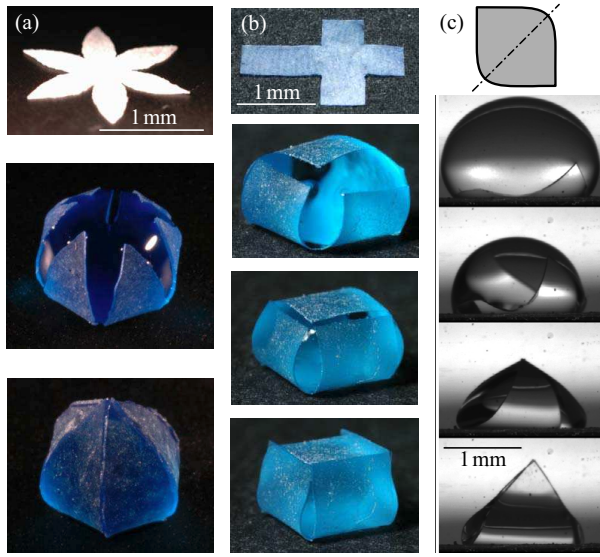


FIG. 5: Tuning the initial shape to obtain (a) a spherical encapsulation, (b) a cubic encapsulation or (c) a triangular mode-2 fold.